Available online at www.sciencedirect.com
SCIENCE DIRECT
Estuarine, Coastal and Shelf Science 69 (2006) 165–178
ESTUARINE COASTAL AND SHELF SCIENCE
www.elsevier.com/locate/ecss

Annual sediment flux estimates in a tidal strait using surrogate measurements

Neil K. Ganju [a,b,*], David H. Schoellhamer [a,b]

[a] U.S. Geological Survey, Placer Hall, 6000 J Street, Sacramento, CA 95819, USA
[b] University of California, Davis, Department of Civil and Environmental Engineering, One Shields Avenue, Davis, CA 95616, USA

Received 9 November 2005; accepted 9 April 2006
Available online 6 June 2006

Abstract

Annual suspended-sediment flux estimates through Carquinez Strait (the seaward boundary of Suisun Bay, California) are provided based on surrogate measurements for advective, dispersive, and Stokes drift flux. The surrogates are landward watershed discharge, suspended-sediment concentration at one location in the Strait, and the longitudinal salinity gradient. The first two surrogates substitute for tidally averaged discharge and velocity-weighted suspended-sediment concentration in the Strait, thereby providing advective flux estimates, while Stokes drift is estimated with suspended-sediment concentration alone. Dispersive flux is estimated using the product of longitudinal salinity gradient and the root-mean-square value of velocity-weighted suspended-sediment concentration as an added surrogate variable. Cross-sectional measurements validated the use of surrogates during the monitoring period. During high freshwater flow advective and dispersive flux were in the seaward direction, while landward dispersive flux dominated and advective flux approached zero during low freshwater flow. Stokes drift flux was consistently in the landward direction. Wetter than average years led to net export from Suisun Bay, while dry years led to net sediment import. Relatively low watershed sediment fluxes to Suisun Bay contribute to net export during the wet season, while gravitational circulation in Carquinez Strait and higher suspended-sediment concentrations in San Pablo Bay (seaward end of Carquinez Strait) are responsible for the net import of sediment during the dry season. Annual predictions of suspended-sediment fluxes, using these methods, will allow for a sediment budget for Suisun Bay, which has implications for marsh restoration and nutrient/contaminant transport. These methods also provide a general framework for estimating sediment fluxes in estuarine environments, where temporal and spatial variability of transport are large.

Keywords: sediment flux; sediment budgets; estuaries; San Francisco Bay

1. Introduction

Sediment supply to a subembayment of an estuary is determined by watershed sediment input and the sediment exchange with adjacent embayments. Sediment supply is a critical variable for investigations of habitat stability, restoration potential, and contaminant fate/transport. Suspended-sediment is needed to create and sustain valuable estuarine habitats such as tidal wetlands (Zedler and Callaway, 2001; Pont et al., 2002; Reed, 2002; Temmerman et al., 2003), though sediment-associated contaminants can also accumulate wherever sediment preferentially deposits (Hornberger et al., 1999; Arzayus et al., 2002; Taylor et al., 2004). In addition, nutrients and biota accumulate near estuarine turbidity maxima (ETM), where high suspended-sediment and contaminant concentrations are found (Peterson et al., 1975; Jassby and Powell, 1994). Enhanced biological activity in these areas may increase contaminant uptake by the food web (Kimmerer et al., 1998).

These issues converge in Suisun Bay, California (Figs. 1 and 2). Over 90% of marsh area has been lost in San Francisco Bay since the 19th century, and current management goals in Suisun Bay include marsh restoration. Deposited sediment

* Corresponding author. U.S. Geological Survey, Placer Hall, 6000 J Street, Sacramento, CA 95819, USA.
E-mail address: nganju@usgs.gov (N.K. Ganju).

0272-7714/$ - see front matter © 2006 Elsevier Ltd. All rights reserved.
doi:10.1016/j.ecss.2006.04.008

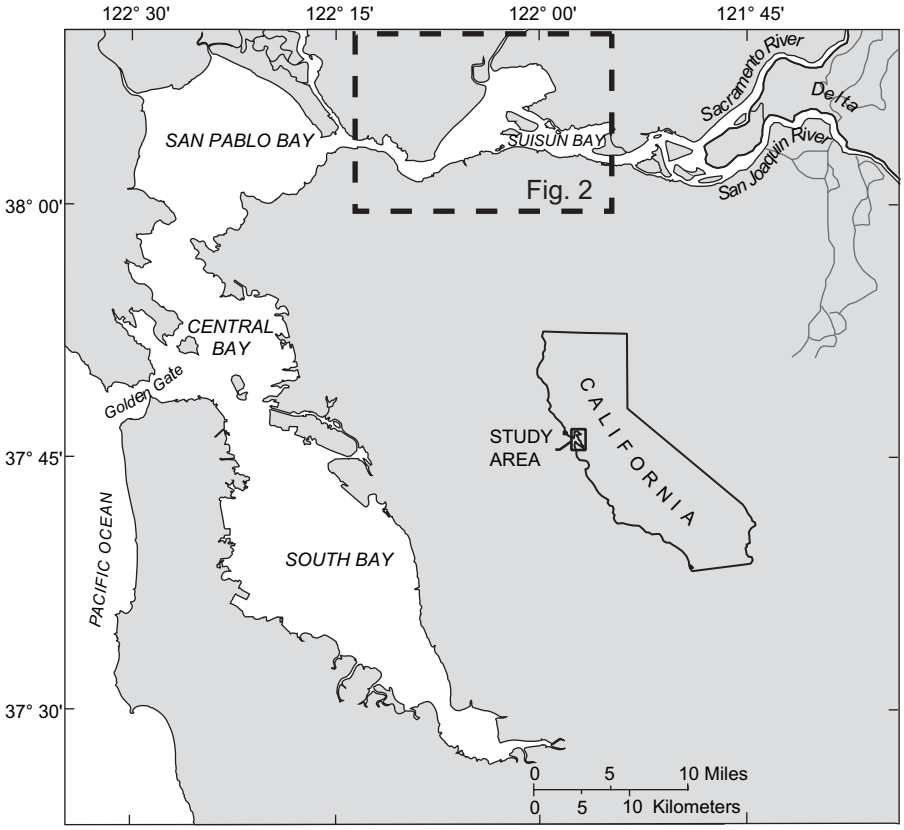

Fig. 1. San Francisco Bay and Sacramento/San Joaquin River Delta. Suisun Bay is the landward-most subembayment of the estuarine system, and receives the majority of its water from the Delta.

in Suisun Bay is thought to be high in mercury concentrations due to 19th century gold mining in the watershed (Hornberger et al., 1999), leading to concerns about resuspension of these deposits over long timescales (>10 yr). Cappiella et al. (1999) show net erosion in Suisun Bay since the first bathymetric surveys in the 19th century. The net sediment budget of Suisun Bay in the current era may shed light on the viability of habitat restoration as well as the magnitude of mercury introduction to the water column. In order to quantify this sediment budget, sediment flux at the landward

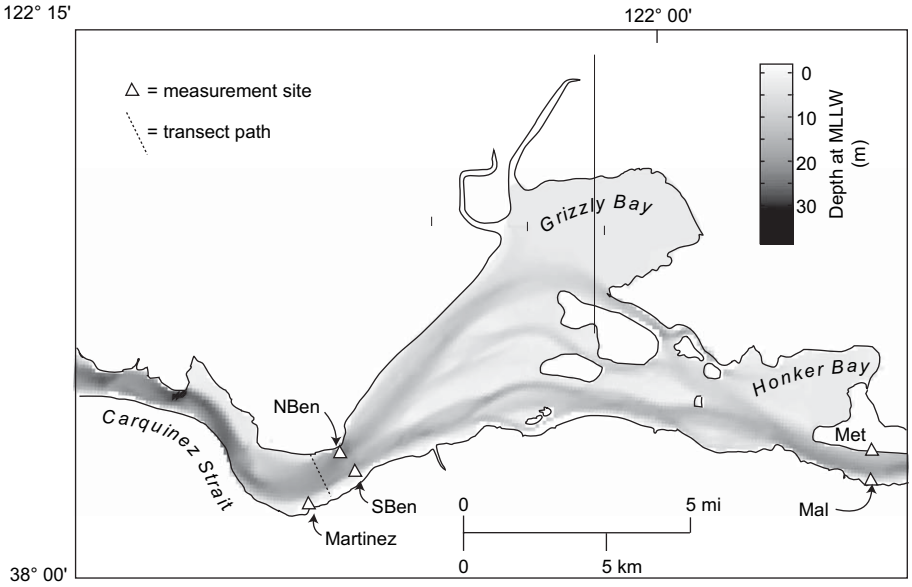

Fig. 2. Suisun Bay outline and bathymetry. Sites Mal and Met are situated at the confluence of the Delta and Suisun Bay. Sites NBen and SBen occupy piers of the Benicia Bridge, landward of Carquinez Strait, which then leads to the expanse of San Pablo Bay.

and seaward boundaries of the subembayment must be determined.

Estimating sediment flux in estuaries can be complicated by the large range of tidal and riverine forcing. Spring and neap tides combined with periods of varying freshwater flow can introduce lateral and vertical variability of suspended-sediment concentrations (SSC) and water velocity. These variations can be induced by salinity gradients, bathymetric forcing, and secondary circulation (Ridd et al., 1998; Blanton et al., 2003). Suisun Bay, as the landward-most subembayment of San Francisco Bay, is subject to variable freshwater flow as well as semi-diurnal tides. The seaward boundary of Suisun Bay is Carquinez Strait, which is approximately 1 km wide and has a maximum depth of 40 m. Formation of an ETM has been noted in Carquinez Strait (due to a sill between Carquinez Strait and Suisun Bay; Jay and Musiak, 1994; Schoellhamer, 2001a), while density stratification has been documented during periods of high and low freshwater flow. The presence of a bend in Carquinez Strait may complicate hydrodynamic conditions.

Proper estimation of suspended-sediment flux through Carquinez Strait must account for the entire cross-section. While monitoring a large cross-section is both physically and financially impossible over the necessary time-frames, it may be possible to identify surrogate data that can be continuously monitored. The use of surrogates in estuaries has previously been explored; Uncles et al. (1998) suggested the use of salinity as a proxy for the location of the turbidity maximum in the Humber–Ouse Estuary, while Warner et al. (2005) used freshwater flow as a surrogate for the longitudinal salinity distribution in the tidal Hudson River. Allen (1990) highlighted the limitations of using marsh accretion rates as a surrogate for sea-level rise, as system characteristics may change over timescales longer than the detailed study periods. In this study, we occupied portions of the channel with autonomous equipment for 3 months, and calibrated those data to tidal-cycle cross-sectional measurements. The results from the 3-month deployment were extrapolated to quantify fluxes over water year 2004, and other years when surrogate data were available.

2. Field observations

2.1. Site description

Suisun Bay spans from the Sacramento/San Joaquin River Delta (Delta) at the landward end to Carquinez Strait at the seaward end. Over one-half of the bay is shallower than 5 m at mean-lower-low-water (MLLW), though numerous deep-water (>10 m) channels run longitudinally through the bay. Two large shallow areas, Grizzly and Honker Bays, lie on the northern edge of the main channels. Maximum depths in Carquinez Strait approach 40 m. The landward end of Carquinez Strait immediately bifurcates at the boundary of Suisun Bay. The northern half of the channel continues northeast into the Reserve Fleet channel and terminates in Grizzly Bay, while the southern half of the channel runs east-northeast along the southern edge of the bay. The two channels are separated by a shallow bar that is partially exposed at low tide.

Freshwater inflow from the Delta is mainly controlled by reservoir releases and water operations within the Delta, and maximum flows are typically in the winter months. Flow is managed to keep the 2-psu isohaline seaward of the Delta during the low-flow season (~May–November). Semi-diurnal tides cause currents exceeding 1 m/s, with a maximum spring tide range in excess of 2 m.

The existing conceptual model (Krone, 1979) suggests that suspended-sediment transport within Suisun Bay follows a seasonal cycle: the majority of suspended-sediment is delivered through the Delta during the large, winter freshwater flows, creating a large pool of erodible sediment within the channels and shallows. During the following summer months reliable onshore winds generate wind-waves, resuspending bed sediments in the shallows for transport by tidal currents. Sediment is most likely transported away from high energy areas (e.g. mudflats, shallow off-channel areas) to lower-energy areas (e.g. continental shelf, marinas, deep channels, marsh surfaces). As the summer progresses, the finer fraction of this erodible pool is reduced. In the fall, when neither wind nor freshwater flow is significant, SSC is at its lowest. As the wet season commences during winter, the cycle repeats itself. Following this model, it has been assumed that Suisun Bay is depositional in the winter, and erosional in the summer.

Previous studies (Burau et al., 1993; Schoellhamer and Burau, 1998) have identified gravitational circulation within Carquinez Strait, especially when the longitudinal salinity gradient is at a maximum. This helps sustain an ETM that forms at the eastern (landward) end of the strait, due to a sharp bathymetric change. This ''sill'', which decreases the depth from 18 m to 11 m, forms a landward control on the gravitational circulation and therefore the ETM (Jay and Musiak, 1994; Schoellhamer, 2001a). Deposition in Carquinez Strait is greatest during neap tides when vertical mixing is minimized and the water column may become stratified. The following spring tides are then able to resuspend the erodible bed sediment and mix the water column. The presence of a bend within channels typically induces secondary circulation patterns. The combination of secondary circulation, density gradients, and bathymetric effects suggests that Carquinez Strait will have a complex cross-sectional pattern of SSC and water velocity. The study was carried out during the spring–summer transition, when the longitudinal salinity gradient should span from its minimum to maximum, and cross-sectional variability may be the most complicated.

2.2. Methods

2.2.1. Spring monitoring period

The U.S. Geological Survey established a continuous monitoring site in the north channel, on the Benicia Bridge in 1997 (site NBen). This site consists of two conductivity, temperature, depth, and optical (nephelometric) sensor multiprobes, at a near-bottom (lower) and a mid-depth (upper) elevation. For this study, a second site was established and maintained

from March 24, 2004 to July 9, 2004 in the south channel (site SBen), also on the Benicia Bridge. Optical backscatter sensors were deployed at the same vertical locations as the multiprobes at site NBen. Fouling and debris interference can reduce data yield from optical sensors, therefore all sensors were cleaned and checked with known standards during site visits (typically once every 3 weeks). Water samples were collected to calibrate the optical sensor output to SSC (Buchanan and Ganju, 2005). Therefore, the four sensors conceptually represent four quadrants of the cross-section: the upper and lower water column of the north channel, and the upper and lower water column of the south channel. The sampling interval was 15 min for all parameters.

Water velocity measurements were collected using two 600 kHz upward-looking acoustic Doppler current profilers (ADCPs), deployed on the bed 300 m seaward of the Benicia Bridge, from March 28, 2004 to July 7, 2004: one in the north channel, and one adjacent to the south channel. Both units were programmed to sample at 10 min intervals, in 0.5 m vertical bins. Total water depth was approximately 16 m at both sites.

2.2.2. Tidal-cycle measurements

Ideally, the true velocity-weighted SSC can be represented by some combination of the SSC values in the four quadrants represented by the four optical sensors. Velocity-weighted SSC in a cross-section is calculated as:

$$\mathrm{SSC}_u = \frac{\int uc \ \mathrm{d}A}{\int u \ \mathrm{d}A} \tag{1}$$

where A is channel area, u and c are velocity and suspended-sediment concentration, respectively, with:

$$u = [u] + u' \tag{2}$$

$$c = [c] + c' \tag{3}$$

Brackets indicate a spatial average value and the prime indicates the spatially fluctuating portion. Eqs. (2) and (3) refer to spatial measurements in the cross-section. If only the spatial average SSC was used (without velocity weighting), the result would ignore the contribution of the non-zero product of $u'c'$ (spatial correlation between velocity and concentration fluctuations). The product of SSC_u and total water discharge (denominator of Eq. (1)) gives total instantaneous sediment flux. Conceptually, if the SSC was not velocity-weighted, then the flux contribution of stagnant water parcels with high SSC would be overestimated, while swift moving parcels with low SSC would be underestimated.

Calibration of the weighting for each of the four quadrants is required because the relative contribution of each quadrant to SSC_u is unknown. Calibration of weights can be accomplished by performing cross-sectional surveys of velocity and SSC. SSC_u can be regressed against the quadrant SSC values, to infer the proper weights for each quadrant. Because obtaining these data is labor-intensive, they are usually collected over short time-frames (<30 h). It was determined that tidal-cycle surveys during a spring and neap tide would be sufficient to characterize variability, based on inspection of previous SSC records at both sites.

Detailed measurements of velocity and SSC were undertaken to estimate SSC_u. Tidal-cycle measurements on June 29, 2004 and July 7, 2004 coincided with neap and spring tides, respectively. Velocities were measured using a boat-mounted 600 kHz ADCP that traversed the channel (1200 m width) every 10–15 min. Conductivity, temperature, depth, and turbidity were measured using a Seabird SBE19plus (any use of trade, product, or firm names is for descriptive purposes only and does not imply endorsement by the U.S. Government) profiling package, deployed from another vessel. This vessel crossed Carquinez Strait every 30–45 min, profiling at 12 nodes in the cross-section. The package was lowered and raised at 1 m/s, sampling at 4 Hz, resulting in a vertical sampling density of 0.25 m. From this same vessel, water samples were collected with a Van Dorn sampler and analyzed for SSC. The corresponding turbidity output from the nearest vertical location and time of the water sample was related to the actual SSC to generate a turbidity-SSC calibration curve. Turbidity output was then converted to SSC using this calibration curve.

All Seabird profiling data were interpolated spatially and temporally to the same transect path, vertical bins, and times of the ADCP measurements. Final interpolated grids were cross-checked with the original Seabird profiles to ensure that errors were not generated in the interpolation process. Therefore, each velocity measurement has a corresponding interpolated SSC value, and SSC_u is calculated using Eq. (1).

2.2.3. Total channel discharge

Total channel discharge for the spring monitoring period was computed via the index-velocity method (Simpson and Bland, 2000). This requires a continuous surrogate for channel-average velocity, namely the index-velocity. The bottom-mounted north channel ADCP provided the index-velocity (depth-averaged velocity). Ideally, both bottom-mounted ADCPs would be considered, but the south channel ADCP data were corrupted and unusable after the unit was tipped over (May 30, 2004). The index-velocity is compared to the channel-average velocity obtained during the tidal-cycle measurements, to provide a rating curve. This curve is then applied to the continuous index-velocity measurements, generating a full time-series of channel-average velocity. Cross-sectional area is computed using the geometry of the cross-section (provided by ADCP measurements), and a stage–area relationship. Continuous stage was measured by the California Department of Water Resources at Martinez. Continuous, instantaneous discharge is calculated as the product of channel-average velocity (obtained from the index-velocity rating) and cross-sectional area (via the stage–area relationship).

2.2.4. Residual suspended-sediment flux calculation

The decomposition of the total constituent flux is given by Dyer (1974). Lateral and vertical variations of SSC in the

channel can be ignored because SSC_u is assumed to account for cross-sectional variability. Thus, the flux equation reduces to:

$$[F] = [U][A][SSC_u] + U'[A][SSC_u] + [U]A'[SSC_u] + U'A'[SSC_u] + [U][A]SSC'_u + U'[A]SSC'_u + [U]A'SSC'_u + U'A'SSC'_u \quad (4)$$

where $[F]$ is the total discharge weighted residual suspended-sediment flux, U is the channel-average velocity, A is the channel area, and SSC_u is the velocity-weighted SSC. Brackets denote a tidally averaged value, while the prime indicates the temporal deviation of the instantaneous value from the tidally averaged value (Eqs. (2) and (3)). Tidal averaging was performed using a low-pass Butterworth filter with a cutoff frequency of $1/30\ h^{-1}$. The filter was applied in the forward and reverse directions to minimize anomalies at the endpoints of the record.

Typically, the advective and dispersive flux terms (Eq. (4), terms 1 and 6, respectively) dominate total flux, while Stokes drift (Eq. (4), term 4) contributes a minor portion. Advective flux quantifies the contribution of mean discharge and mean concentration (e.g. river flow), while dispersive flux represents the correlation between velocity and concentration fluctuations. Stokes drift accounts for the correlation of velocity and area, which is landward for a progressive tidal wave. The remaining terms are usually negligible.

2.2.5. Annual sediment flux estimation

Predicting fluxes in Carquinez Strait over a year or more requires the use of surrogate measurements that are simpler to obtain than the labor-intensive measurements detailed above. The available surrogates that are continuously measured are QWEST (combined discharge from four sites within the Delta; Oltmann, 1998), and lower SSC at site NBen (Buchanan and Ganju, 2005). Upper SSC was not used due to a lower data return. An additional surrogate that delineates the high-flow from the low-flow regime is the difference in salinity between Carquinez Strait and Mallard Island (longitudinal salinity gradient; LSG), which can have a strong influence on local hydrodynamics and sediment transport (Monismith et al., 1996). The quantities that must be predicted are advective $[U][A][SSC_u]$, dispersive $U'[A]SSC'_u$, and Stokes drift flux $U'A'[SSC_u]$. The relationship between calculated fluxes and the surrogate variables will be investigated.

2.2.6. Yearly sediment budgets for Suisun Bay

Once the predictive capabilities outlined above are developed, they provide an estimate of net suspended-sediment flux through the seaward boundary of Suisun Bay. Flux estimates for the landward boundary of Suisun Bay are provided by the methods of McKee et al. (in press). Combining the estimates from these boundaries yields a sediment budget for Suisun Bay. Bedload transport and minor tributary sediment fluxes are considered negligible (Porterfield, 1980). This sediment budget does not include changes in storage caused by dredging and sand mining.

3. Results

3.1. Spring monitoring period

Point SSC in the four quadrants was successfully measured for the duration of the spring monitoring period, though fouling and debris decreased the percentage of valid data (Fig. 3). At site NBen, SSC data yield was 79% and 94% for the upper and lower sensors, respectively. Data yield at site SBen was 64% and 91% for the upper and lower sensors, respectively. SSC was elevated at all sites near the beginning of the record, due to recent sediment supply from the Delta, overlapping with a spring tide.

Inspection of the time-series data (Fig. 3) reveals substantial lateral and vertical variability in SSC. At both sites, mean SSC at the lower sensor was over twice that of the upper sensor. On a tidal timescale, the water column was relatively well-mixed on strong tides, though on weak flood and weak ebb tides during increased freshwater flow (April 6–April 29, 2004), stratification was evident. The density stratification during this time inhibited vertical mixing, and this stratification was disrupted on the following strong tide. Laterally, SSC at site SBen was maximum at flood tide, while site NBen experienced elevated SSC on ebb tides as well. The north channel is directly connected on the landward side to the expanse of Grizzly Bay, which has elevated SSC following spring runoff (Krone, 1979; Warner et al., 2004), while the south channel is not directly connected to any shallow embayments.

Velocity data at site NBen were obtained for the entire deployment, while the instrument at site SBen was tipped over on May 30, 2004, leading to a loss of the data for the remainder of the deployment. Velocity data at site NBen show a marked ebb-dominance, while the flood-dominance at site SBen is pronounced in the lower water column.

3.2. Tidal-cycle measurements

The tidal-cycle, cross-sectional measurements validate the large lateral and vertical variability observed in the time-series of point SSC. On early ebb tide, velocity in the northern half of the channel led the southern half, which was still slightly flooding. As the entire channel turned to ebb, SSC was greatest on the northern edge of the channel (Fig. 4A). The transition from ebb to flood was characterized by increasing landward velocity in the lower water column in the south channel, while water in the north channel continued to ebb. This led to a core of high velocity and maximum SSC near the bottom of the south channel. As flood tide progressed, the high velocity region began to spread laterally and vertically. Maximum SSC was still found near the bottom in the south channel, but suspended-sediment began to increase near the bottom in the north channel as well (Fig. 4B).

SSC_u ranged from 65 to 187 mg/L, at slack before ebb and early flood tide, respectively. SSC data were interpolated to the same location of velocity data, in order to calculate SSC_u in the cross-section (Eq. (1)). Multiple linear regression

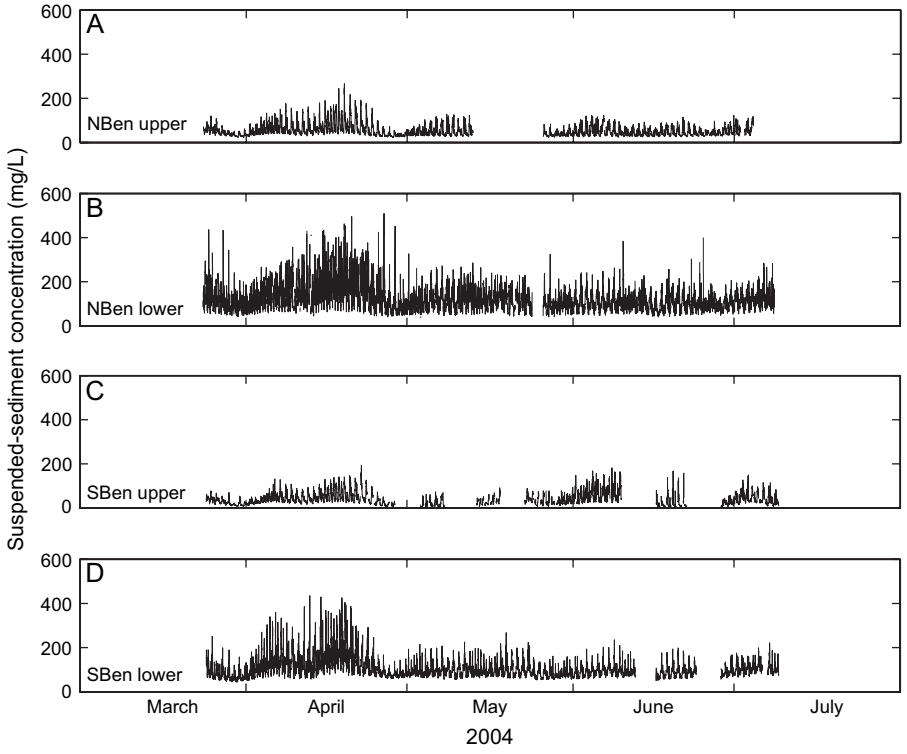

Fig. 3. Suspended-sediment concentration (SSC) time-series from sites (A) upper sensor at site NBen; (B) lower sensor at site NBen; (C) upper sensor at site SBen; and (D) lower sensor at site SBen. Note higher data return from lower sensors (tiles B, D). SSC was typically higher at lower sensors.

was used for separate flood and ebb calibrations (Fig. 5A), with lower sensor SSC at sites NBen and SBen as the independent variables, and SSC_u as the dependent variable. The continuous time-series of SSC_u (Fig. 6B) was created by applying the flood and ebb regressions to the individual sensor data. The SSC_u time-series retains the features from both sensors, which capture the lateral variation in SSC between flood and ebb tide.

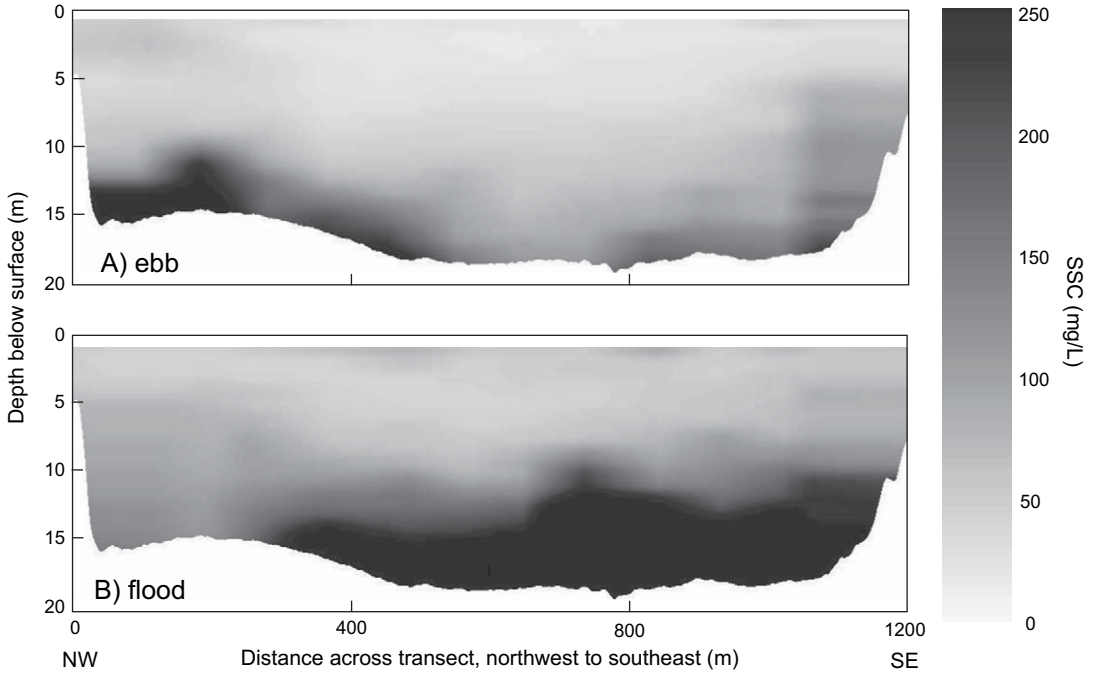

Fig. 4. Interpolated profiles of suspended-sediment concentration. Early ebb profile (A) shows higher concentrations in the ebb-dominant north channel, while SSC is maximized in the south channel at the beginning of flood (B). Maximum SSC in each profile is 320 and 1000 mg/L, respectively.

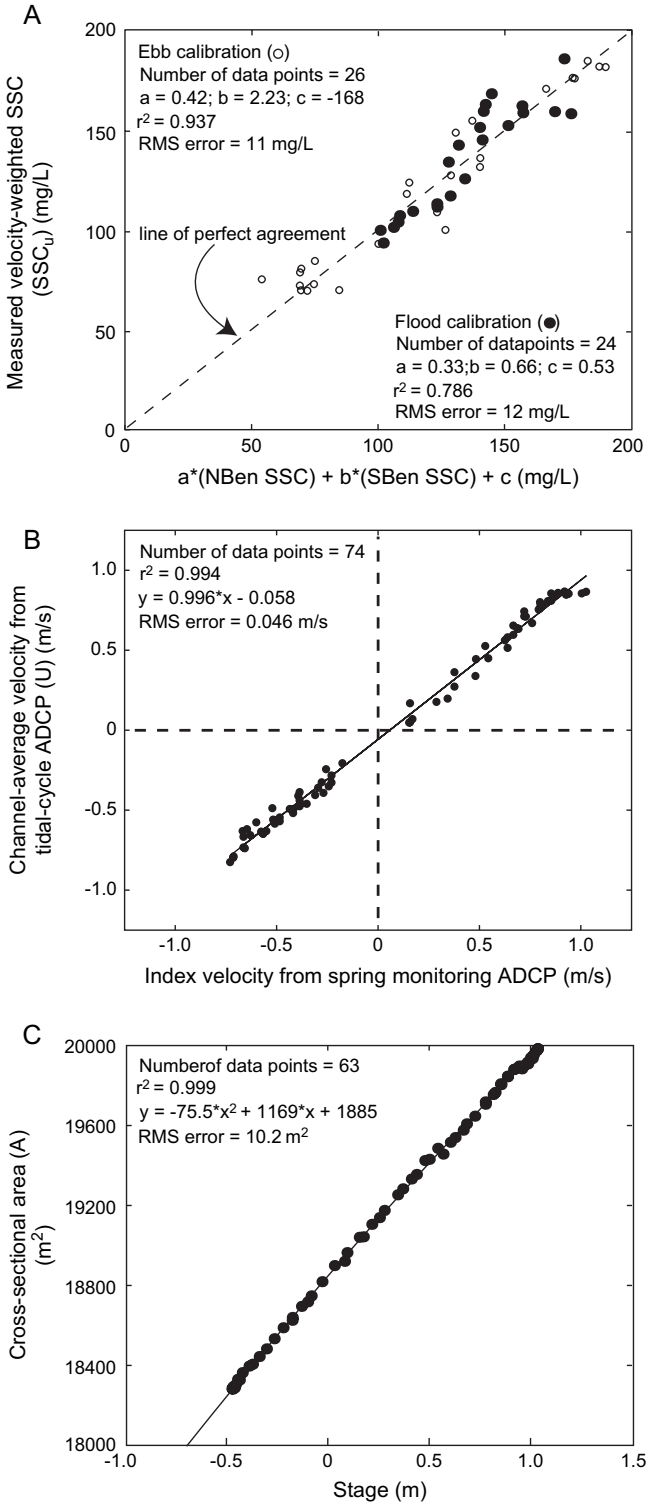

Fig. 5. Regression analysis used for calibration of (A) site NBen and SBen SSC to velocity-weighted SSC (SSC_u); (B) index-velocity to channel-average velocity (U); and (C) stage to cross-sectional area (A). Tidal-cycle measurements were used to obtain relationships that can be extended over spring monitoring period, yielding advective ($[U][A][SSC_u]$), dispersive $\left(U'[A]\left[SSC'_u\right]\right)$, and Stokes drift ($U'A'[SSC_u]$) fluxes over the spring monitoring period.

3.3. Total channel discharge

The index-velocity method (Fig. 5, tiles B, C) provides continuous channel-average velocity and channel cross-sectional area, and therefore continuous discharge (Fig. 6A). The accuracy of the discharge record was evaluated in comparison with QWEST and Dayflow (California Department of Water Resources, 2005), which suggested that the estimated discharge had a slight flood bias (Q_{original}, Fig. 7). Dayflow is an idealized, unidirectional flow value that is the net water balance of all freshwater inputs and outputs to the Sacramento/San Joaquin River Delta. Due to the large cross-sectional area at the measurement site, a 1 cm/s flood bias in velocity is enough to negate a freshwater flow of 180 m^3/s, which is 50% of the mean Dayflow magnitude during the spring monitoring period. Therefore, QWEST and Dayflow were used as bounds to validate a 1 cm/s (22% of RMS error; Fig. 5B) ebb-directed shift of the velocity data to represent freshwater flow adequately. Other possible sources and sinks of water were investigated, including groundwater seepage and evaporation. Aquifer exchange in San Francisco Bay can be both upward and downward, but maximum downward seepage rates are 0.55 m/yr (Spinelli et al., 2002). Assuming this maximum seepage rate over the entire area of Suisun Bay (169 million m^2) yields a water volume loss of 3 m^3/s, which is negligible. Maximum evapotranspiration rates in the area were 0.007 m/d; the product of this vertical water loss and the area of Suisun Bay yields a total volume loss of 14 m^3/s, which is not enough to account for the discrepancy. While the measurement of instantaneous discharge is difficult in large cross-sections, a bias in flow measurement at high-flows is negligible, and at low-flows the advective water flux is minimal nonetheless. The bias has no effect on dispersive fluxes, because the tidally averaged trend in water discharge is subtracted when calculating that quantity.

The time-series of instantaneous (Q) and tidally averaged ($[Q]$) discharge (Fig. 6A) demonstrate the tidal and subtidal variability of discharge through Carquinez Strait. The mostly positive (ebb-directed) magnitude of tidally averaged discharge represents the net freshwater flow delivered through the Delta. During low freshwater flow periods (Fig. 6A, post-April 29, 2004), residual discharge is more influenced by the spring/neap cycle, and meteorological effects such as wind and barometric pressure (Tobin et al., 1995), though it is still ebb-dominated due to continuous reservoir releases. The direction of the residual discharge can turn landward (Fig. 6A, June 3–7, 2004) during periods of sustained onshore winds, though tidal forcing can also have a similar effect.

3.4. Flux calculation

Advective, dispersive, and Stokes drift flux components accounted for 98% of the total flux. Advective flux of sediment was predominantly in the seaward direction, while dispersive flux was mainly directed landward (as was Stokes

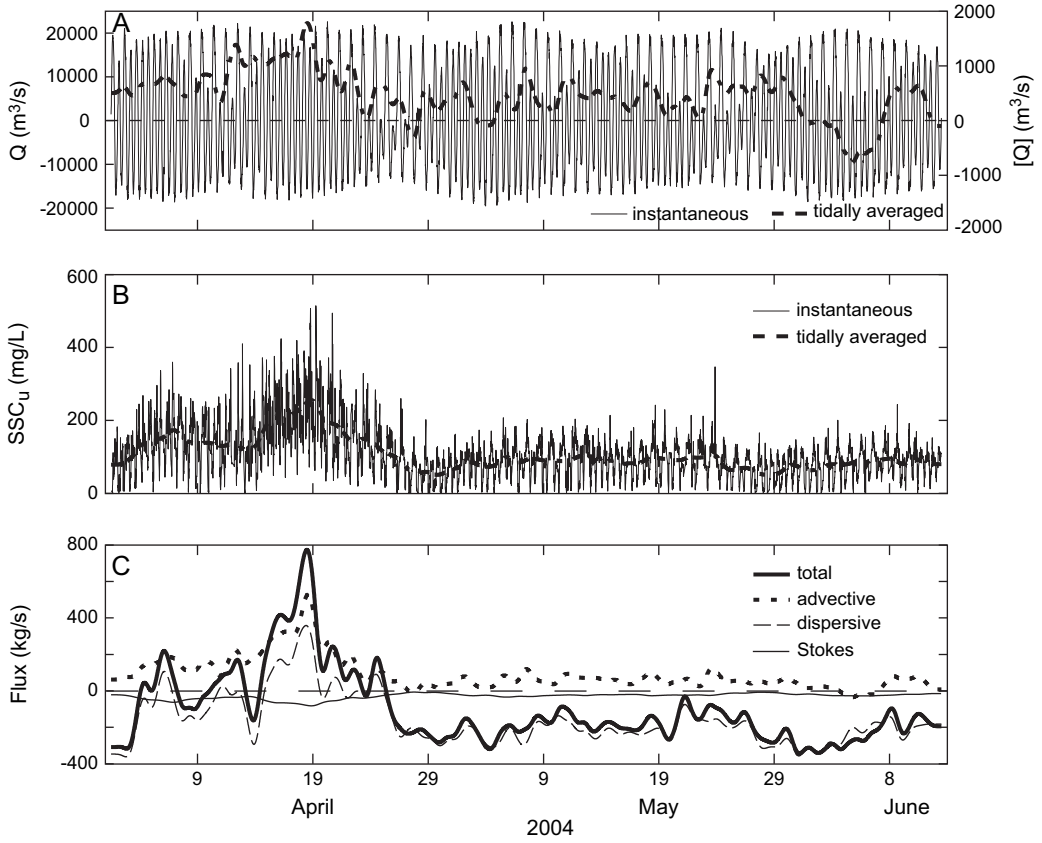

Fig. 6. Tile (A) instantaneous (Q) and tidally averaged discharge ([Q]) in Carquinez Strait (shifted, see Fig. 7); (B) velocity-weighted suspended-sediment concentration, SSC_u; and (C) total, advective, dispersive, and Stokes drift flux components. Positive values indicate seaward (ebb) transport, negative values indicate landward (flood) transport.

drift). Exceptions did occur, however: dispersive flux turned seaward during a period of sustained freshwater flow (April 9–19, 2004; Fig. 6, tiles A, C), and advective flux was directed landward during a period of increased westerly winds (June 3–7, 2004). After freshwater flow returned to typical summer conditions (post-April 29, 2004), advective flux was minimal, while dispersive flux dominated transport.

Advective flux by definition follows the residual water flux, and increasing river flows usually correspond with increasing advective flux. The Stokes drift flux is a direct function of tidally averaged SSC_u, and therefore was maximized when tidally averaged SSC_u was a maximum. The dispersive flux measures the correlation between tidal velocity fluctuations and SSC_u, and the landward direction during low-flow can be attributed to the coincident profiles of velocity and SSC. Over the spring monitoring period, the direction of residual near-bed velocity (from the upward-looking ADCPs) was typically landward, while the direction was seaward near the top of the water column; this is commonly known as gravitational circulation and has been previously identified in Carquinez Strait. Combining landward residual near-bed velocity with high near-bed SSC (as compared to low near-surface SSC) results in a net landward flux of suspended-sediment in the Strait during low freshwater flow.

3.5. Annual sediment flux estimation

The first term of Eq. (4) is the advective flux, which is composed of the product of $[U][A]$ and $[SSC_u]$. Estimating $[U][A]$ (advective water discharge) requires a surrogate measurement,

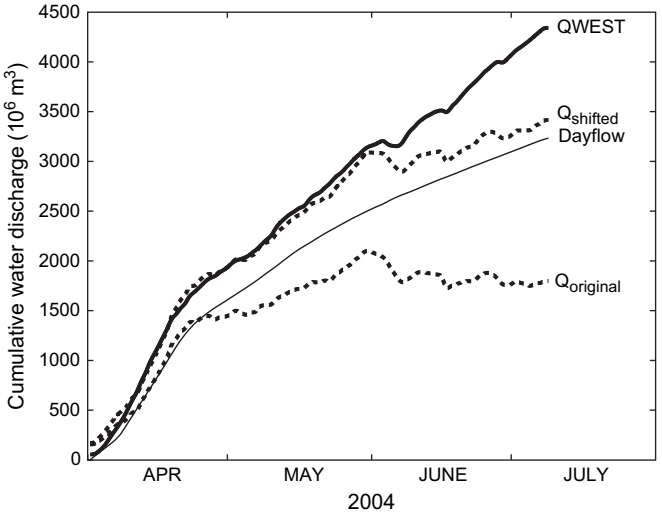

Fig. 7. Cumulative water discharge calculated from Delta measurement sites (QWEST), Dayflow, discharge measured in Carquinez Strait ($Q_{original}$), and $Q_{original}$ with 1 cm/s ebb-directed shift ($Q_{shifted}$).

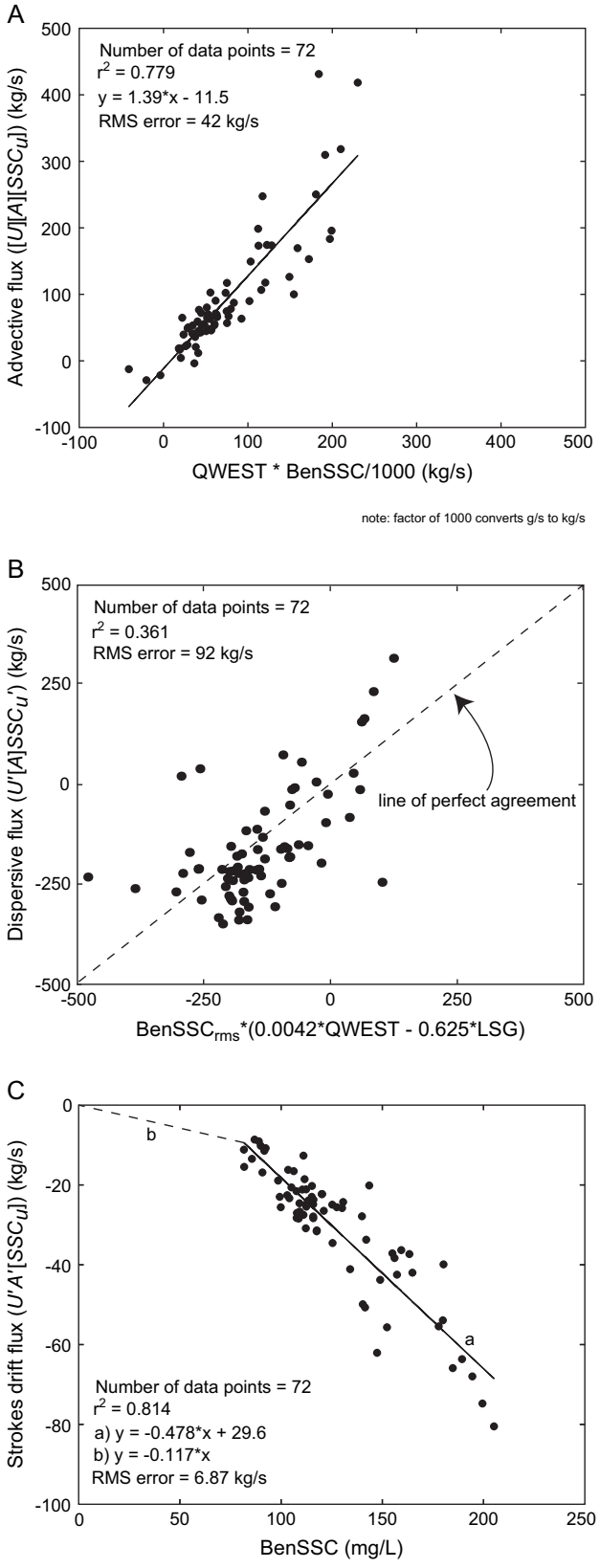

and we use the continuously monitored, tidally averaged discharge through the Delta (QWEST). Water losses between the Delta and Carquinez Strait are assumed to be negligible, as evaporation, groundwater input/output, and surface water withdrawals are minimal. [SSC_u] is replaced with the tidally averaged lower SSC from site NBen, which is measured continuously. While the intratidal dynamics of SSC at site NBen are different than the southern half of the channel (site SBen), using the tidally averaged value avoids this discrepancy. The product of QWEST and BenSSC yields a surrogate for advective flux, which is regressed against the directly calculated value to provide a calibration curve (Fig. 8A) and predictions for the spring monitoring period (Fig. 9B).

Estimating dispersive flux requires accounting for wet and dry season dynamics. From the spring monitoring results, dispersive flux was seaward during periods of high seaward advective flux, but turned landward as freshwater flow and seaward advective flux decreased. This transition occurred in concert with the return of salinity to Suisun Bay. Therefore, QWEST represents the wet season dynamics, while the salinity in Suisun Bay represents the dry season dynamics. As one regression variable we use the product of longitudinal salinity gradient, LSG (salinity difference between Carquinez Strait and Mallard Island), in Suisun Bay and an estimate of the fluctuating suspended-sediment concentration, $BenSSC_{rms}$, defined as:

$$\mathrm{BenSSC_{rms}} = \sqrt{\left[(\mathrm{BenSSC}')^2\right]} \tag{5}$$

A multiple linear regression using the product (LSG)($BenSSC_{rms}$) and the product (QWEST)($BenSSC_{rms}$) as independent variables is suitable for predicting dispersive flux (Fig. 8B; Fig. 9C). Seaward dispersive flux is maximized during high seaward advective flux and low salinity gradient periods, while landward dispersive flux is maximized during periods of low seaward (or significant landward) advective flux, high salinity gradient, and high $BenSSC_{rms}$.

The use of $BenSSC_{rms}$ is preferred over BenSSC because large flow events may raise BenSSC while the fluctuations are minimal. In water year 2004, for example, a 4500 m^3/s freshwater flow event (February 20, 2004) raised BenSSC, but $BenSSC_{rms}$ was minimal. Therefore, dispersive flux should be minimized at that time. Conversely, a 1700 m^3/s flow event (April 9, 2004) that coincided with a spring tide induced large BenSSC, and large $BenSSC_{rms}$. Increases in SSC due to wind-

Fig. 8. Comparison of fluxes obtained from measurements with developed surrogates; (A) Linear regression of QWEST and lower SSC at site NBen (BenSSC) product to advective flux; (B) multiple linear regression of RMS value of lower SSC at site NBen ($BenSSC_{rms}$), QWEST, and longitudinal salinity gradient (LSG) versus dispersive flux; and (C) lower SSC at site NBen (BenSSC) to Stokes drift flux. Regression is extended to zero to avoid seaward Stokes drift flux (regression *b*). Advective, dispersive, and Stokes drift fluxes calculated during spring monitoring period (Fig. 5) were used to obtain relationships that can be extended over all times where surrogates (QWEST, site NBen SSC, longitudinal salinity gradient) are available, yielding advective, dispersive, and Stokes drift flux estimates over those same periods.

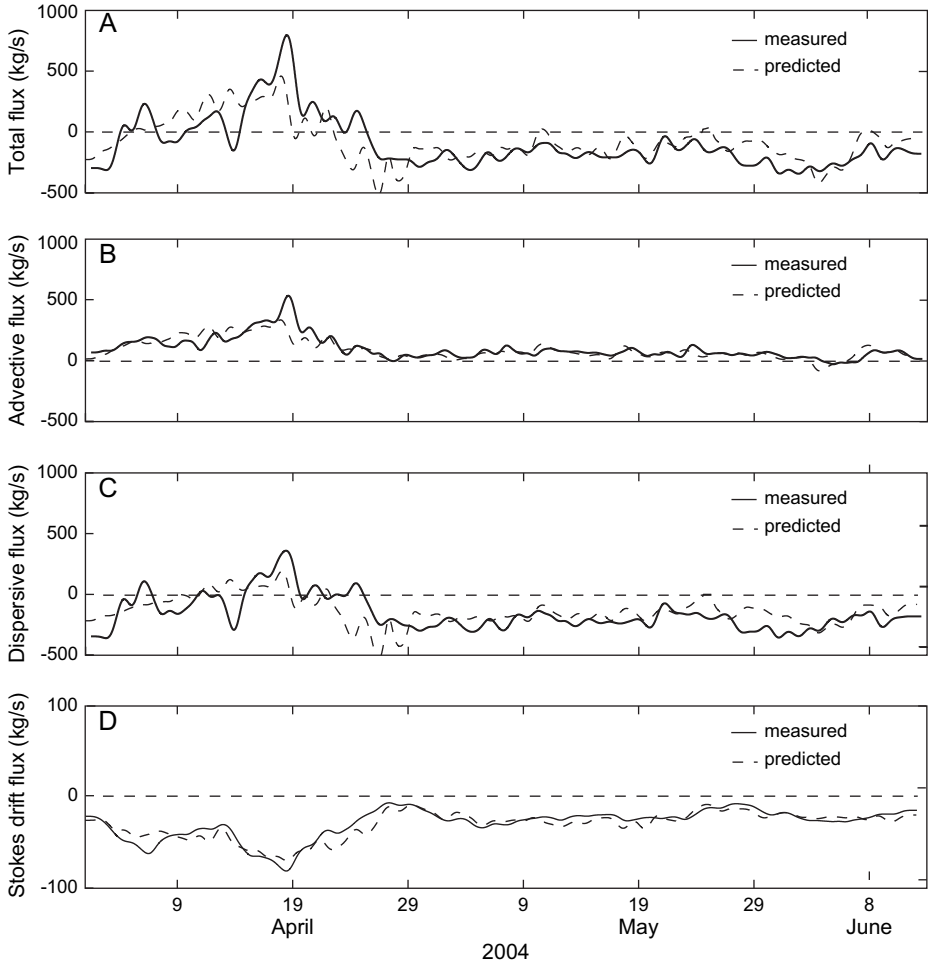

Fig. 9. Spring monitoring period measured and predicted fluxes; (A) total flux (sum of advective, Stokes drift, and dispersive flux); (B) advective flux; (C) dispersive flux; and (D) Stokes drift flux. Positive values indicate seaward (ebb) transport, negative values indicate landward (flood) transport.

wave resuspension in San Pablo Bay (which has extensive shallow regions) are also accounted for by using $\mathrm{BenSSC_{rms}}$.

Improved predictions of dispersive flux ($r^2 = 0.70$) were achieved by allowing for an intercept or by decoupling $\mathrm{BenSSC_{rms}}$ from LSG, but the functionality of those relations erroneously allow for large landward dispersive fluxes when LSG is high and $\mathrm{BenSSC_{rms}}$ is at a minimum. Therefore, goodness-of-fit is sacrificed for improved conceptual functionality. Stokes drift flux is adequately predicted using BenSSC alone as a surrogate for $[\mathrm{SSC}_u]$ in Eq. (4), term 4 (Fig. 8C; Fig. 9D). While the correlation of velocity and area are neglected, Stokes drift is adequately represented with SSC alone.

3.6. Yearly sediment budgets for Suisun Bay

Yearly predictions of sediment fluxes through Suisun Bay demonstrate large variability, because the years considered are also highly variable in terms of freshwater flow (Table 1). The data suggest that extremely wet years promote sediment export, while dry years restrict seaward advective transport, and large landward dispersive flux dominates. The only year with seaward dispersive flux is 1998, which had persistent freshwater flow and low salinity gradient through most of the summer months. The prolonged freshwater flow season possibly decreased the strength of gravitational circulation between San Pablo Bay and Suisun Bay. High SSC through the summer combined with substantial freshwater flow lead to the large export flux. The error involved with the dispersive flux prediction is larger than advective and Stokes drift flux predictions (Fig. 8), therefore differences in total dispersive flux between water years may not be significant. However, the net direction of these fluxes is clearly modulated by residual flow and sediment concentrations, as an extreme year such as 1998 demonstrates.

4. Discussion

4.1. Accuracy of long-term prediction

The extrapolation of relations developed during the transition between wet and dry season introduces errors of an unknown magnitude, but this does not change the seasonal pattern of suspended-sediment transport. The most intensive measurement period was conducted during tidal-cycles in

Table 1
Cumulative flow and estimated fluxes for water years where surrogate data are available. Positive values indicate seaward transport

Water year	Cumulative water flow (m^3)	Sediment flux: Mallard Island (Mt)	Sediment flux: Carquinez Strait (Mt)	Net sediment budget (Mt)	Advective flux (Mt)	Dispersive flux (Mt)	Stokes drift flux (Mt)
1997	42.3×10^9	2.24	5.07	2.83 (export)	9.13	−3.15	−0.92
1998	53.6×10^9	2.42	20.93	18.51 (export)	13.00	8.94	−1.01
2002	11.3×10^9	0.309	−2.803	3.11 (import)	1.02	−3.51	−0.32
2003	17.3×10^9	0.546	0.167	0.379 (import)	2.30	−1.68	−0.45
2004	17.9×10^9	0.619	0.612	0.006 (import)	2.70	−1.56	−0.53

June and July 2004, when freshwater flow was minimized and salinity gradient was at a maximum. Those efforts result in relations for channel-average velocity, channel cross-sectional area, and velocity-weighted SSC (tidal-cycle measurements) as a function of index-velocity, stage, and point SSC values (spring monitoring measurements). Errors in this procedure include the error of the index-velocity method (Simpson and Bland, 2000), and the error of the velocity-weighted SSC calibration. Potential error arose from a flood-biased velocity in the index-velocity calibration, however, a shift of the velocity data (22% of RMS error) was applied based on two independent measurements of freshwater flow.

Variability in hydrodynamic conditions, specifically freshwater flow and density stratification, may cause these low-flow ratings to be invalid during periods of higher freshwater flow. Therefore, the generality of these ratings was investigated with the Regional Oceanic Modeling System (ROMS; Shchepetkin and McWilliams, 2005). The domain of Suisun Bay was modeled using tidal forcing in Carquinez Strait, freshwater flow from the Delta, and a synthetic time-series of suspended-sediment (Schoellhamer, 2001b) at the western boundary of Carquinez Strait. The model was calibrated to stage, and validated with vertical and longitudinal salinity dynamics (Ganju and Schoellhamer, submitted for publication). The calibration of index-velocity to channel-average velocity was nearly identical between the modeled low-flow and high-flow period of 2004, suggesting that the calibration developed from field measurements should be applicable during high-flow periods. The prediction of velocity-weighted SSC was performed in the same manner as detailed in Section 3.2, using model results for velocity-weighted SSC, and SSC at sites NBen and SBen. A regression developed for the low-flow period of 2004 had errors of 15% and 9% for ebb and flood, respectively; applying that regression to the high-flow period of 2004 increased errors to 17% and 11%. These small increases in error suggest that the use of low-flow ratings for all periods is reasonable.

From this a continuous record of fluxes was developed for the spring monitoring period, and those calculated fluxes were then related to three surrogate variables: lower sensor SSC at site NBen, longitudinal salinity gradient, and QWEST. The regression errors indicated can only be estimated for the period of calibration, and extrapolation of these relations over higher freshwater flow events may introduce further error. RMS error for the respective flux components was 44% of mean advective flux, 48% of mean dispersive flux, and 22% of mean Stokes drift flux. Errors in the dispersive flux prediction are larger in magnitude than the other flux components, but goodness-of-fit is sacrificed for conceptual quality. Despite the limitations of these procedures, the predictive methods here can be refined by additional cross-sectional surveys of velocity and SSC during periods of major and minor freshwater flow. Because the surrogates (site NBen SSC, QWEST, and longitudinal salinity gradient) are continuously measured, periodic surveys can check the validity of the relationships developed here, and extend relations into other regimes.

4.2. Dispersive flux prediction

The results of the spring monitoring period suggested that dispersive flux was maximized in the seaward direction during high-flow (with the caveat that $BenSSC_{rms}$ is high), while landward dispersive flux is maximized when salinity gradient is maximized. The basis for this analysis is the gravitational circulation mechanism: when flow is large, the longitudinal salinity gradient is compressed in Carquinez Strait, and landward flux due to gravitational circulation is restricted. When flows are reduced, the salinity gradient expands and landward flux commences. This simplistic treatment ignores the underlying complexity of the interaction between flow, salinity gradient, and gravitational circulation. For instance, the local salinity gradient may be very different than the basin-scale salinity gradient. Measurements during the spring monitoring period show that salinity gradient is compressed in Carquinez Strait during high-flows, and expanded within Suisun Bay. Conversely, during low-flows the salinity gradient is expanded in Carquinez Strait, and compressed in Suisun Bay. We have chosen the basin-scale measurement here (salinity gradient from site Mal to site NBen) because we are estimating sediment fluxes through Carquinez Strait and into Suisun Bay. If we were aspiring to understand the local sediment flux within Carquinez Strait itself, the local salinity gradient would be of more interest. There still remains uncertainty in utilizing point values to calculate salinity gradients, as complex bathymetries and channel configurations suggest vertical and horizontal structure to the salinity field. Nonetheless, for the bulk predictions made here, the pattern of salinity gradient between two boundary points should provide adequate representation of the average salinity dynamics.

4.3. Seasonal pattern of erosion and deposition

Previous researchers (e.g. Krone, 1979) have speculated that winter freshwater flows replenish the erodible sediment pool on the bed of Suisun Bay, while the wind-dominated summer periods allow for erosion and reduction of this sediment pool. Our measurements suggest the opposite pattern, at least under present watershed sediment yield conditions. For the water years considered here, the largest freshwater flood brought relatively little sediment past the Mallard Island boundary as compared to historic conditions (McKee et al., in press). This essentially creates a clear-water flow condition, and combined with the relatively high residual SSC in the water column, this results in a net export of sediment from Suisun Bay during the wet season.

Once freshwater flow subsides to typical dry season conditions, wind-wave resuspension begins to mobilize sediment throughout San Francisco Bay. Wind-wave resuspension is a major factor for increasing SSC in both Suisun and San Pablo Bay; however, 224 million m^2 of San Pablo Bay are shallower than 5 m, while only 97 million m^2 of Suisun Bay fit this criterion (Jaffe et al., 1998; Cappiella et al., 1999). Therefore, wind-wave resuspension has a greater effect in San Pablo Bay, creating a gradient in SSC from west to east. This leads to a landward dispersive flux, as flood tide carries relatively higher SSC than ebb tide. The two-layer flow which has been observed in Carquinez Strait also promotes landward sediment flux, since near-bottom residual currents directed landward would coincide with higher near-bottom SSC, and seaward residual surface currents coincide with lower surface SSC. The exception to this pattern is water year 1998, which had persistent freshwater flow during the summer.

Water years with different hydrographs (Table 1) suggest different patterns: water year 1997 witnessed a large net seaward advective flux and large net landward dispersive flux, with a pattern similar to water year 2004. However, in water year 1998, net dispersive flux was large and seaward. Despite the similar cumulative flow between water years 1997 and 1998, the increased residual flows throughout the summer in water year 1998 (due to reservoir releases) led to a low salinity gradient and persistent seaward advective flux through the normally ''dry'' season. The traditional wind-wave resuspension pattern during the summer, combined with increased residual flow, results in persistent export during the summer. In both years, Suisun Bay exported suspended-sediment, despite large watershed sediment fluxes (McKee et al., in press). The five water years considered here are extreme conditions (mean $= 28.5 \times 10^9$ m^3, standard deviation $= 18.4 \times 10^9$ m^3) and represent years when a reasonable percentage of data were available. Further data collection during several water years will assist interpretation.

4.4. Ramifications of sediment flux patterns

The suspended-sediment budget of Suisun Bay has major ramifications for marsh vertical dynamics and sustainability. The fringing marshes of Suisun Bay depend on surface deposition during high water when suspended-sediment is introduced in the overlying water, and deposited due to low horizontal velocities within the marsh canopy. The rate of sediment supply to Suisun Bay, whether from the watershed (via the Delta) or seaward embayments (San Pablo Bay), is a critical factor for marsh sustainability, especially in light of sea-level rise. These results suggest sediment transport at the boundaries of Suisun Bay is highly variable on a yearly basis, though redistribution within Suisun Bay cannot be quantified by this study.

The exchange of sediment between San Pablo Bay and Suisun Bay shows that nutrients and contaminants can be introduced to Suisun Bay from San Pablo Bay. In addition, there is clearly a seasonal pattern. High concentrations of contaminants (e.g. mercury, polycyclic aromatic hydrocarbons) have been measured in the sediments of San Pablo Bay and Suisun Bay, and exchange between them shows that toxic sources in a seaward embayment can impact the water quality in a landward embayment. Contaminant and nutrient uptake rates among various species are frequently dependent on the season (e.g. Linville et al., 2002), and the seasonal exchange pattern may shed light on the importance of exposure periods.

In terms of the sediment budget for Suisun Bay, it is clear that San Pablo Bay must be an important source of sediment. Jaffe et al. (1998) show that San Pablo Bay was net depositional between 1856 and 1951, until the last measurement period (1951–1983) which showed net erosion. By comparison, Suisun Bay had a peak erosional period between 1922 and 1942, and during the last measurement period (1942–1990) that erosion rate had reduced. This may reflect a redistribution of sediment between the two subembayments, as they are still responding to the perturbation of hydraulic mining in the mid-1800's. If San Pablo Bay has an excess of bed sediment (i.e. out of balance with the erosional force supplied by wind waves and currents), and Suisun Bay has a corresponding deficit, there should be a transferal of sediment from San Pablo Bay, either seaward or landward. Assuming that some portion of that excess can be transferred landward during low freshwater flow periods, Suisun Bay would be the recipient.

Major floods export large quantities of sediment and cause net erosion within the basin, while dry periods allow for sediment import from seaward embayments, and resulting deposition. Frequency and magnitude of floods may determine whether Suisun Bay is erosional or depositional on decadal timescales. In light of global climate change affecting regional temperatures (and therefore snowpack in the watershed), the timing and magnitude of freshwater flows to Suisun Bay may change significantly in this century (Knowles and Cayan, 2002). Larger flow events earlier in the season may greatly alter temporal erosion and deposition patterns, as the summer phase of landward delivery of sediment is further separated from the sediment export phase in the spring.

5. Conclusions

Despite the highly variable nature of velocity, salinity, and SSC in estuarine cross-sections, reasonable measurements of

suspended-sediment flux can be made over limited periods. Ideally, these measurements can be related to continuously monitored surrogates. Such a procedure was performed for Carquinez Strait, California, the seaward boundary of Suisun Bay. The calculated fluxes show a clear pattern of seasonality to the advective and dispersive fluxes; these patterns suggest that down-estuary subembayments are major sources of sediment to lower-energy landward embayments, especially when watershed sediment fluxes to the landward embayment are negligible. Predictions for several water years indicate that Suisun Bay exports sediment during the wet season, and imports sediment from San Pablo Bay, the seaward embayment, during the dry season. The exception to this is water year 1998, when persistent freshwater flows were observed during the summer. The seasonal sediment flux pattern may be due to a trend of sediment redistribution from San Pablo Bay (which was depositional between 1856 and 1951, but erosional between 1951 and 1983) to Suisun Bay (where erosion rate has been decreasing since 1942). Net sediment transport to and from Suisun Bay has major implications for marsh restoration and nutrient/contaminant transport in the entire San Francisco Bay. Exchanges of sediment-associated contaminants and nutrients are clearly important between embayments, and are not simply one-way processes from watershed to ocean.

Acknowledgments

This work was paid for in part with funds from California State Water Resources Control Board contract #01-281-150-2. Tidal-cycle measurements were performed with the assistance of Curt Battenfeld, Greg Brewster, Paul Buchanan, Jay Cuetara, Megan Lionberger, Heather Ramil, Greg Shellenbarger, and Brad Sullivan. ADCP data were analyzed by Randal Dinehart. Catherine Ruhl provided Delta flow data and advice. Jon Burau supplied invaluable input concerning the hydrodynamics of the area. Jan Thompson, Jessica Lacy, and the two anonymous reviewers provided helpful reviews of the manuscript.

References

Allen, J.R.L., 1990. Constraints on measurement of sea-level movements from salt-marsh accretion rates. Journal of the Geological Society 147, 5–7.

Arzayus, K.M., Dickhut, R.M., Canuel, E.A., 2002. Effects of physical mixing on the attenuation of polycyclic aromatic hydrocarbons in estuarine sediments. Organic Geochemistry 33, 1759–1769.

Blanton, J.O., Seim, H., Alexander, C., Amft, J., Kineke, G., 2003. Transport of salt and suspended sediments in a curving channel of a coastal plain estuary: Satilla River, GA. Estuarine, Coastal and Shelf Science 57, 993–1006.

Buchanan, P.A., Ganju, N.K., 2005. Summary of suspended-sediment concentration data in San Francisco Bay, California, water year 2003. U.S. Geological Survey Data Series 113.

Burau, J.R., Simpson, M.R., Cheng, R.T., 1993. Tidal and residual currents measured by an acoustic Doppler current profiler at the west end of Carquinez Strait, San Francisco Bay, California, March to November 1988. U.S. Geological Survey Water-Resources Investigations Report 92-4064, 79 pp.

California Department of Water Resources, 2005. DAYFLOW program documentation and DAYFLOW data summary user's guide. http://iep.water.ca.gov/dayflow.

Cappiella, K., Malzone, C., Smith, R., Jaffe, B., 1999. Sedimentation and bathymetry changes in Suisun Bay, 1867–1990. U.S. Geological Survey Open-File Report 99-563.

Dyer, K.R., 1974. The salt balance in stratified estuaries. Estuarine and Coastal Marine Science 2, 273–281.

Ganju, N.K., Schoellhamer, D.H. Lateral displacement of the estuarine turbidity maximum in tidal strait. Proceedings of the Eighth International Conference on Cohesive Sediment Transport, Saga, Japan, September 20–23, submitted for publication.

Hornberger, M.I., Luoma, S.N., van Geen, A., Fuller, C., Anima, R., 1999. Historical trends of metals in the sediments of San Francisco Bay, California. Marine Chemistry 64, 39–55.

Jaffe, B.E., Smith, R.E., Torresan, L.Z., 1998. Sedimentation and bathymetric change in San Pablo Bay, 1856–1983. U.S. Geological Survey Open-File Report 98–759.

Jassby, A.D., Powell, T.M., 1994. Hydrodynamic influences on interannual chlorophyll variability in an estuary: upper San Francisco Bay–Delta (California, U.S.A.). Estuarine, Coastal and Shelf Science 39, 595–618.

Jay, D.A., Musiak, J.D., 1994. Particle trapping in estuarine turbidity maxima. Journal of Geophysical Research 99, 446–461.

Kimmerer, W.J., Burau, J.R., Bennett, W.A., 1998. Tidally oriented vertical migration and position maintenance of zooplankton in a temperate estuary. Limnology and Oceanography 43, 1697–1709.

Knowles, N., Cayan, D., 2002. Potential effects of global warming on the Sacramento/San Joaquin watershed and the San Francisco estuary. Geophysical Research Letters 29 (18), 1891. doi:10.1029/2001GL014339.

Krone, R.B., 1979. Sedimentation in the San Francisco Bay system. In: Conomos, T.J. (Ed.), San Francisco Bay: The Urbanized Estuary. Pacific Division of the American Association for the Advancement of Science, San Francisco, California, pp. 85–96.

Linville, R.G., Luoma, S.N., Cutter, L., Cutter, G.A., 2002. Increased selenium threat as a result of invasion of the exotic bivalve *Potamacorbula amurensis* into the San Francisco Bay–Delta. Aquatic Toxicology 57, 51–64.

McKee, L., Ganju, N.K., Schoellhamer, D.H. Estimates of suspended sediment flux entering San Francisco Bay from the Sacramento and San Joaquin Delta, San Francisco Bay, California. Journal of Hydrology, in press.

Monismith, S., Burau, J.R., Stacey, M., 1996. Stratification dynamics and gravitational circulation in northern San Francisco Bay. In: Hollibaugh, J.T. (Ed.), San Francisco Bay: The Ecosystem. Pacific Division of the American Association for the Advancement of Science, San Francisco, pp. 123–153.

Oltmann, R.N., 1998. Indirect measurement of Delta outflow using ultrasonic velocity meters and comparison to mass-balance calculated outflow. Interagency Ecological Program Newsletter 11, 5–8.

Peterson, D.H., Conomos, T.J., Broenkow, W.W., Doherty, P.C., 1975. Location of the non-tidal current null zone in northern San Francisco Bay. Estuarine and Coastal Marine Science 3, 1–11.

Pont, D., Day, J.W., Hensel, P., Franquet, E., Torre, F., Rioual, P., Ibanez, C., Coulet, E., 2002. Response scenarios for the deltaic plain of the Rhone in the face of an acceleration in the rate of sea-level rise with special attention to *Salicornia*-type environments. Estuaries 25 (3), 337–358.

Porterfield, G., 1980. Sediment transport of streams tributary to San Francisco, San Pablo, and Suisun Bays, California, 1909–1966. U.S. Geological Survey Water Resources Investigations 80–64, 92 pp.

Reed, D.J., 2002. Understanding tidal marsh sedimentation in the Sacramento–San Joaquin Delta, California. Journal of Coastal Research Special Issue 36, 605–611.

Ridd, P.V., Stieglitz, T., Larcombe, P., 1998. Density-driven secondary circulation in a tropical mangrove estuary. Estuarine, Coastal and Shelf Science 47, 621–632.

Schoellhamer, D.H., 2001a. Influence of salinity, bottom topography, and tides on locations of estuarine turbidity maxima in northern San Francisco Bay. In: McAnally, W.H., Mehta, A.J. (Eds.), Coastal and Estuarine Fine Sediment Transport Processes. Elsevier Science B.V., pp. 343–357.

Schoellhamer, D.H., 2001b. Singular spectrum analysis for time series with missing data. Geophysical Research Letters 28 (16), 3187–3190.

Schoellhamer, D.H., Burau, J.R., 1998. Summary of findings about circulation and the estuarine turbidity maximum in Suisun Bay, California. U.S. Geological Survey Fact Sheet FS-047-98, 6 pp.

Shchepetkin, A.F., McWilliams, J.C., 2005. The Regional Ocean Modeling System (ROMS): a split-explicit, free-surface, topography-following coordinates ocean model. Ocean Modelling 9, 347–404.

Simpson, M.R., Bland, R., 2000. Methods for accurate estimation of net discharge in a tidal channel. Institute of Electrical and Electronics Engineers Journal of Oceanic Engineering 25, 437–445.

Spinelli, G.A., Fisher, A.T., Wheat, C.G., Tryon, M.D., Brown, K.M., Flegal, A.R., 2002. Groundwater seepage into northern San Francisco Bay: implications for dissolved metal budgets. Water Resources Research 38 (7). doi:10.1029/2001WR000827.

Taylor, S.E., Birch, G.F., Links, F., 2004. Historical catchment changes and temporal impact on sediment of the receiving basin, Port Jackson, New South Wales. Australian Journal of Earth Sciences 51, 233–246.

Temmerman, S., Govers, G., Meire, P., Wartel, S., 2003. Modelling long-term tidal marsh growth under changing tidal conditions and suspended sediment concentrations, Scheldt estuary, Belgium. Marine Geology 193, 151–169.

Tobin, A., Schoellhamer, D.H., Burau, J.R., 1995. Suspended-solids flux in Suisun Bay, California. In: Proceedings of the First International Conference on Water Resources Engineering. San Antonio, Texas, pp. 1511–1515.

Uncles, R.J., Joint, I., Stephens, J.A., 1998. Transport and retention of suspended particulate matter and bacteria in the Humber–Ouse Estuary, United Kingdom, and their relationship to hypoxia and anoxia. Estuaries 21 (4A), 597–612.

Warner, J.C., Geyer, W.R., Lerczak, J.A., 2005. Numerical modeling of an estuary: a comprehensive skill assessment. Journal of Geophysical Research 110, C050001. doi:10.1029/2004JC002691.

Warner, J.C., Schoellhamer, D.H., Ruhl, C.A., Burau, J.R., 2004. Floodtide pulses after low tides in shallow subembayments adjacent to deep channels. Estuarine, Coastal and Shelf Science 60, 213–228.

Zedler, J.B., Callaway, J.C., 2001. Tidal wetland functioning. Journal of Coastal Research Special Issue 27, 38–64.